Civil Engineering Infrastructures Journal, 51(2): 425 – 443, December 2018
Print ISSN: 2322-2093; Online ISSN: 2423-6691
DOI: 10.7508/ceij.2018.02.011

Impact of Integration on Straining Modes and Shear-Locking for Plane Stress Finite Elements

Badrkhani Ajaei, B.[1] and Ghassemieh, M.[2*]

[1] Ph.D. Candidate, Department of Civil Engineering, Bogazici University, Bebek, Istanbul, Turkey.
[2] Professor, School of Civil Engineering, College of Engineering, University of Tehran, Tehran, Iran.

Received: 19 Feb. 2018; Revised: 04 Jul. 2018; Accepted: 07 Jul. 2018

ABSTRACT: Stiffness matrix of the four-node quadrilateral plane stress element is decomposed into normal and shear components. A computer program is developed to obtain the straining modes using adequate and reduced integration. Then a solution for the problem of mixing straining modes is found. Accuracy of the computer program is validated by a closed-form stiffness matrix, derived for the plane rectangular as well as square element. It is shown that method of integration has no effect on the straining modes, but it influences the eigenvalues of the bending modes. This effect is intensified by increasing the element aspect ratio, confirming the occurrence of shear locking.

Keywords: Finite Elements, Plane Stress, Reduced Integration, Shear Locking, Straining Modes.

INTRODUCTION

Straining modes of an element are used to represent the forms of deformation that the element exhibits. The straining modes are especially important for ensuring convergence of the Finite Element solution. Previous research in the field of straining modes of plane stress elements (Bathe, 2014; Pawsey and Clough, 1971), provide contradicting results, and the complexities of the eigenvalue problem are not reported in these studies.

Shear-locking, a condition in which the resistance of the element to bending loads is greatly overestimated is caused by the inability of the element to experience the expected bending deformations subjected to the specific conditions. Different approaches are taken to overcome the shear-locking problem. Rezaiee-Pajand and Yaghoobi (2013) defined shear-locking as an inevitable consequence of choosing a polynomial formulation for strain field, and defined parasitic shear as a similar type of element stiffening resulting from presence of normal strain terms in the shear strain interpolation function. The authors mentioned reduced integration as a way to counter the parasitic shear problem, and not the shear-locking. Rezaiee-Pajand and Yaghoobi (2017) developed a new type of plane quadrilateral element by using separate strain field formulations for the boundaries and the interior of the element. The developed element had nodes with both translational and

* Corresponding author E-mail: m.ghassemieh@ut.ac.ir

rotational degrees of freedom; and was immune to parasitic shear. Several different elements available in the literature or developed by the authors were compared by performing numerical tests by Rezaiee-Pajand and Yaghoobi (2015).

Shear-locking has been the subject of many research works. Many researchers (e.g. Bletzinger et al., 2000; Nguyen-Thanh et al., 2008; Nguyen-Xuan et al., 2010; da Veiga et al., 2012) have focused on developing elements immune to shear-locking. Fallah et al. (2017) explained the shear-locking quandary in thin plate elements, and proposed a new type of plate element that solved that problem in a computationally efficient way. Others have used strategies to alleviate the shear-locking problem, for instance using absolute nodal coordinates (Garcia-Vallejo et al., 2007). There is also research to overcome shear-locking in numerical methods other than Finite Element method (Kanok-Nukulchai et al., 2001). Research in shear-locking includes plane elements (Rezaiee-Pajand and Yaghoobi, 2014), plate bending elements (Pugh et al., 1978), and shell elements (Arnold and Brezzi, 1997).

The distinction between shear-locking and parasitic shear is not always made in the literature, and reduced integration is usually introduced as a way of encountering shear-locking. Reddy (1997) mentioned reduced integration as a way to eliminate shear-locking in beam elements. Also Pugh et al. (1978) showed that reduced integration can be an effective tool for mitigating the shear locking problem in quadrilateral plate elements.

It is a conventional practice to evaluate the performance of elements by solving examples of simple assemblies (e.g. cantilever beam, curved beam, etc.), an approach adopted by some research papers including (Rezaiee-Pajand and Yaghoobi, 2014). One problem with that approach is that it is not possible to test the element for every possible combination of geometry, meshing, and loading configurations.

However, in this research, we take an alternative approach. The eigen-analysis approach adopted in this research paper is based on the concept of element straining modes as described by Pawsey and Clough (1971) and by Bathe (2014). This Eigen-analysis approach addresses the problem in a more direct way, by looking into the capability of the element itself to experience certain basic deformation shapes (e.g. expansion-contraction, elongation, shearing, etc.).

Evaluating Finite Elements using eigenvalue analysis has been suggested by previous research (e.g. Bathe, 2014; Pawsey and Clough, 1971). However, to the knowledge of the authors, a detailed method of applying selective integration to plane stress elements in not given. This research uses Hamilton's principle (Liu and Quek, 2014) to separate the stiffness matrix of a quadrilateral plane stress element to shear and normal parts, providing a method of selective integration. The problem of shear-locking is analyzed from an Eigen-analysis perspective, and the effectiveness of reduced integration is studied.

The method of separating the stiffness matrix is applicable to Finite Element simulations using general quadrilateral plane stress and plane stress elements. For applying the method of reduced integration, one needs to perform numerical integration on the shear and bending parts of the element stiffness separately. However, for a membrane plane stress element, each node has two translational degrees of freedom, and do not have shear and bending degrees of freedom similar to bending beam elements.

In this paper, a method of separating the shear and bending portions of the stiffness matrix of a four-node quadrilateral plane stress element is proposed. Subsequently, a computer program is developed that

calculates the stiffness matrices of the aforementioned elements using normal and reduced integration methods. The straining modes of a square shaped element are obtained using the developed computer program. Repeated Eigen values result in mixing of straining modes. This problem is solved by changing the dimensions of the element slightly. The straining modes obtained by the proposed method are a selection of the straining modes reported in the literature, including the straining modes reported by Bathe (2014), shown in figure1. An element with higher aspect ratio is also studied in order to investigate the correlation between straining modes and shear-locking.

STRAINING MODES

The deformations that an element is able to represent can be determined by solving the eigenvalue problem of the following equation:

$$[K_e]\{\phi\} = \lambda\{\phi\} \tag{1}$$

where $[K_e]$: is the element's stiffness matrix, λ is a scalar, and $\{\Phi\}$: is a vector with the dimension equivalent to the number of degrees of freedom of the element. Solving Eq. (1) would result in different values for λ, which are called eigenvalues. For each eigenvalue λ_i, there is a corresponding vector $\{\Phi_i\}$, called eigenvector, which can be calculated by substituting λ_i for λ in Eq. (1). The eigenvectors obtained by Eq. (1) correspond to the nodal displacements of different straining shapes in which an element is able to deform (Bathe, 2014).

For the four-node quadrilateral plane stress element discussed in this paper, these deformation shapes comprise three rigid body motion modes, and five straining modes. These straining modes are presented in (Bathe, 2014; Pawsey and Clough, 1971). Figure 1 shows the straining modes given by Bathe (2014). The straining modes presented in Pawsey and Clough (1971) is slightly different from these straining modes. The stretching and uniform extension modes are replaced by two constant strain modes, and the flexural modes have a trapezoidal shape, and are called bending modes. Presence of these different straining modes in eigenvectors of the stiffness matrix formulation of an element is essential for the convergence of the Finite Element solution by refining the mesh (Bathe, 2014).

STIFFNESS MATRIX

In this section, the stiffness matrix of the four-node quadrilateral plane stress element is presented. Then the reduced integration with the decomposition of the stiffness matrix is discussed.

Existing Formulation of the Element Stiffness Matrix

The four-node quadrilateral plane stress element is shown in Figure 2. The strain vector $\{\varepsilon\}$ has three components being the two normal strains and one shear strain, as shown by the following equation:

$$\{\varepsilon\} = \begin{Bmatrix} \varepsilon_x \\ \varepsilon_y \\ \gamma_{xy} \end{Bmatrix} \tag{2}$$

Moreover, the strain vector can be associated to the nodal displacements $\{d\}$; via strain–displacement transformation relation; as follows:

$$\{\varepsilon\} = [B]\{d\} \tag{3}$$

where $[B]$: is called the gradient matrix, and it consists of the derivatives of interpolation functions of the element with respect to the coordinates. As explained in detail in (Logan, 2012; Liu and Quek, 2014), for plane elements with constant thickness, the element

stiffness matrix can be obtained by the following:

$$[K_e] = t\int_{A_e} [B]^T [D][B] dA \tag{4}$$

where A_e: is the area of the element, and dA: is the area increment.

For general quadrilateral element, it is easier to perform the integration in Eq. (4) after mapping the element into a square domain defined by the natural coordinates, ζ and η of the element which is shown in Figure 3. Therefore, the stiffness matrix of the quadrilateral element in the natural coordinates is defined as following:

$$[K_e] = t\int_{-1}^{1}\int_{-1}^{1} [B]^T [D][B] J \left| d\zeta . d\eta \right. \tag{5}$$

where t: is the element thickness, and [D]: is the constitutive material matrix for the plane stress problem defined by the following equation:

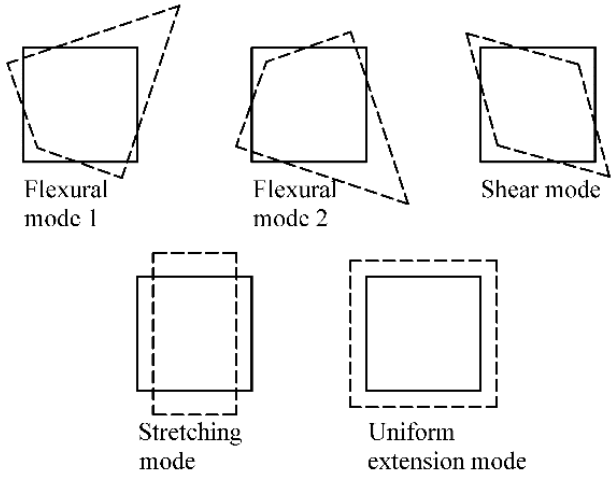

Fig. 1. Straining modes given by Bathe (2014)

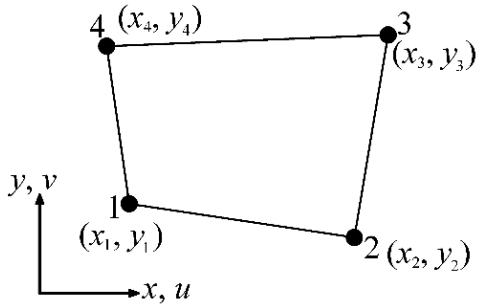

Fig. 2. Four-node quadrilateral plane stress element

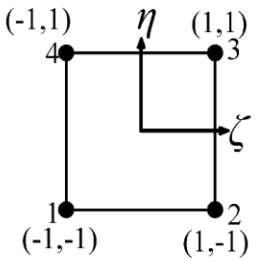

Fig. 3. Natural coordinate system of the element

$$[D]=\begin{cases}\dfrac{E}{1-\nu^2}\begin{bmatrix}1 & \nu & 0\\ \nu & 1 & 0\\ 0 & 0 & \dfrac{1-\nu}{2}\end{bmatrix} & \text{(for plane stress)}\\ \dfrac{E}{(1+\nu)(1-2\nu)}\begin{bmatrix}1-\nu & \nu & 0\\ \nu & 1-\nu & 0\\ 0 & 0 & \dfrac{1-2\nu}{2}\end{bmatrix} & \text{(for plane strain)}\end{cases} \quad (6)$$

where E: is the young's modulus and ν: is the poisson's ratio of the material, whereas $|J|$: is the Jacobian determinant which is defined by:

$$|J|=\begin{vmatrix}\dfrac{\partial x}{\partial \zeta} & \dfrac{\partial y}{\partial \zeta}\\ \dfrac{\partial x}{\partial \eta} & \dfrac{\partial y}{\partial \eta}\end{vmatrix} \quad (7)$$

It should be noted that [B] in Eq. (5) is defined in the natural coordinates of the element, and a simplified way to calculate it, is given by Logan (2012). There is no straightforward closed form solution of Eq. (5) for a general quadrilateral element. Symbolic computation methods can be used for deriving exact solutions for any particular element (Videla et al., 2008; Walentyski, 2007). However, the most common integration method used in the Finite Element method of analysis is the Gauss-Quadrature method (Logan, 2012). For the case of one dimensional integration, n Gaussian integration points provide the exact solution of the integral of the polynomial with the order of $2n$-1 or less (Kreyszig, 2011). Usually, for solving Eq. (5) for a four-noded quadrilateral plane stress element, one needs to employ two-point Gauss integrations for each axis of the natural coordinate system. We call this method of integration normal or adequate integration.

Reduced Integration

Using Normal Gaussian integration for evaluating the stiffness matrix can lead to a condition named shear-locking in certain conditions. Shear-locking is a result of inability of the employed interpolation functions to capture the real deformations of an element in certain conditions of geometry or loading; and results in overestimation of stiffness matrix (Reddy, 2006). Shear-locking is not a problem specific to plane stress elements. This problem happens similarly in shell elements with linear displacement fields (Zienkiewicz et al., 1971). As it was shown in Javidinejad (2012), geometry of structure and meshing techniques can result in elements with high aspect ratios, which may experience shear locking. In fact, the general problem of locking is observed in different kind of elements (Adam, et al., 2014; 2015; Pagani et al., 2014). For a plane stress quadrilateral element, shear-locking can be avoided by using a lower order Gaussian integration for the shear strain energy of the element (Pawsey and Clough, 1971). For a four-node element, this corresponds to using a single Gauss point. This method of integration, which employs different integration techniques for normal and shear strain energies, is called reduced integration or selective integration.

Application of reduced integration may lead to undesirable numerical problems including omission of the correct modes (Rezaiee-Pajand and Yaghoobi, 2012, 2013), and should be used with caution. The objective of this research paper is not to promote reduced integration method, but to objectively see its effects on the straining capabilities of the element and its potential for shear-locking.

Decomposing the Stiffness Matrix for Reduced Integration

The stiffness matrix calculated by Eq. (5) does not have separate components for the stiffnesses resulted by shear strain energy and normal strain energy. Consequently, to perform reduced integration, a change in the formulation is required. Hence, an alternative approach to derive the stiffness is used, which separates the terms of shear and normal strain energy.

One can decompose the strain vector presented in Eq. (2) as sum of two vectors; as follows:

$$\{\varepsilon\} = \{\varepsilon_n\} + \{\varepsilon_s\} \tag{8}$$

where $\{\varepsilon_n\}$: is the normal strain component vector and $\{\varepsilon_s\}$: is the shear strain component vector; as follows:

$$\{\varepsilon_n\} = \begin{Bmatrix} \varepsilon_x \\ \varepsilon_y \\ 0 \end{Bmatrix} \tag{9}$$

and

$$\{\varepsilon_s\} = \begin{Bmatrix} 0 \\ 0 \\ \gamma_{xy} \end{Bmatrix} \tag{10}$$

Similar to Eq. (3), the normal and shear strain vectors can be related to the nodal displacements $\{d_e\}$ by the following equations:

$$\{\varepsilon_n\} = [B_n]\{d_e\} \tag{11}$$

$$\{\varepsilon_s\} = [B_s]\{d_e\} \tag{12}$$

where $[B_n]$: is obtained by substituting the third row of the gradient matrix $[B]$ by zeros and $[B_s]$: is found by substituting the first two rows of the gradient matrix $[B]$ by zeros.

The elastic strain energy of the element is defined by the following:

$$\Pi_e = \frac{1}{2}\int_{V_e} \{\varepsilon\}^T [D]\{\varepsilon\} dV \tag{13}$$

where V_e: is the volume of the element, and dV: is an infinitesimal volume.

Similarly, one can obtain the normal strain energy Π_n^e resulted by the normal strains and the shear strain energy Π_s^e by the following equations:

$$\Pi_n^e = \frac{1}{2}\int_{V_e} \{\varepsilon_n\}^T [D]\{\varepsilon_n\} dV \tag{14}$$

$$\Pi_s^e = \frac{1}{2}\int_{V_e} \{\varepsilon_s\}^T [D]\{\varepsilon_s\} dV \tag{15}$$

Furthermore, the total strain energy can be written as:

$$\Pi_e = \Pi_n^e + \Pi_s^e \tag{16}$$

Substituting Eqs. (14-15) in Eq. (16), and then substituting $\{\varepsilon_n\}$ and $\{\varepsilon_s\}$ by Eqs. (11-12), one can obtain the total strain energy; as follows:

$$\begin{aligned} \Pi_e = &\frac{1}{2}\int_{V_e} \{d_e\}^T [B_n]^T [D][B_n]\{d_e\} dV \\ &+ \frac{1}{2}\int_{V_e} \{d_e\}^T [B_s]^T [D][B_s]\{d_e\} dV \end{aligned} \tag{17}$$

The integrations in Eq. (17) are performed on the coordinates, and because the nodal displacements are degrees of freedom then the above equation is rewritten as:

$$\begin{aligned} \Pi_e = &\frac{1}{2}\{d_e\}^T \left(\int_{V_e} [B_n]^T [D][B_n] dV\right)\{d_e\} \\ &+ \frac{1}{2}\{d_e\}^T \left(\int_{V_e} [B_s]^T [D][B_s] dV\right)\{d_e\} \end{aligned} \tag{18}$$

Eq. (18) can be rewritten as:

$$\Pi_e = \frac{1}{2}\{d_e\}^T [K_n^e]\{d_e\} + \frac{1}{2}\{d_e\}^T [K_s^e]\{d_e\} \quad (19)$$

where

$$[K_n^e] = \int_{V_e} [B_n]^T [D][B_n] dV \quad (20)$$

and

$$[K_s^e] = \int_{V_e} [B_s]^T [D][B_s] dV \quad (21)$$

Hamilton's principle (Liu and Quek, 2014) states that of all admissible displacements, the most accurate displacement field makes the Lagrangian functional stationary (minimum). This leads to the variational equation of the following:

$$\delta \int_{\tau_1}^{\tau_2} L.d\tau = 0 \quad (22)$$

where $d\tau$: is the time increment, τ_1 and τ_2: are representing the time domains, δ: is the operator of variation, and L: is the Lagrangian functional; which in the case of static analysis is defined as:

$$L = -\Pi_e + W_f \quad (23)$$

where Π_e: is the elastic strain energy which can be obtained by Eq. (19), and W_f: is the work done by the external forces, and can be calculated by:

$$W_f = \{d_e\}^T \{F_e\} \quad (24)$$

where $\{F_e\}$: is the vector of the equivalent nodal forces. Substituting Eqs. (19) and (24) in Eq. (23) and then in Eq. (22), one can obtain the following:

$$\delta \int_{\tau_1}^{\tau_2} (-\frac{1}{2}\{d_e\}^T [K_n^e]\{d_e\} - \frac{1}{2}\{d_e\}^T [K_s^e]\{d_e\} + \{d_e\}^T \{F_e\}).d\tau = 0 \quad (25)$$

Using a property of the variation, the above equation can be rewritten as:

$$\delta\left(\{d_e\}^T\right)\int_{\tau_1}^{\tau_2} (-[K_n^e]\{d_e\} - [K_s^e]\{d_e\} + \{F_e\}).d\tau = 0 \quad (26)$$

Since the term δ ($\{d_e\}^T$) has an arbitrary value, Eq. (26) demands the term inside the integral to be zero. This results in the following:

$$([K_n^e] + [K_s^e])\{d_e\} = \{F_e\} \quad (27)$$

The expression inside the parenthesis is the stiffness matrix of the element by definition. This is expressed by:

$$[K_e] = [K_n^e] + [K_s^e] \quad (28)$$

where $[K_n^e]$ and $[K_s^e]$: are defined by Eqs. (20-21), and represent the stiffness of the element resulted from the normal and shear strain energies; and can be subjected to different integration methods. For a four-node plane stress element with constant thickness, the increment of volume in Eqs. (20-21) equals to the thickness t of the element multiplied by the area increment (dA being dx times dy). Transforming Eqs. (20-21) from global coordinates (x-y) to the natural coordinates (ζ-η), the following equations are obtained for the isoparametric formulation of the element:

$$[K_n^e] = t\int_{-1}^{1}\int_{-1}^{1} [B_n]^T [D][B_n] |J| d\zeta.d\eta \quad (29)$$

and

$$[K_s^e] = t\int_{-1}^{1}\int_{-1}^{1} [B_s]^T [D][B_s] |J| d\zeta.d\eta \quad (30)$$

All the equations derived here for decomposing the stiffness matrix are also valid for the plane strain case.

CLOSED FORM SOLUTION FOR THE RECTANGULAR ELEMENT

As mentioned in last sections, there is no straightforward closed form solution for the stiffness matrix of the general quadrilateral element shown in Figure 2. However, for a rectangular element like the one shown in Figure 4, the closed form solution can easily be obtained.

The matrix [*B*] of Eq. (3) for this element is given as Eq. (31):

$$[B]=\frac{1}{4bh}\begin{bmatrix} y-h & 0 & h-y & 0 & h+y & 0 & -h-y & 0 \\ 0 & x-b & 0 & -b-x & 0 & b+x & 0 & b-x \\ x-b & y-h & -b-x & h-y & b+x & h+y & b-x & -h-y \end{bmatrix} \tag{31}$$

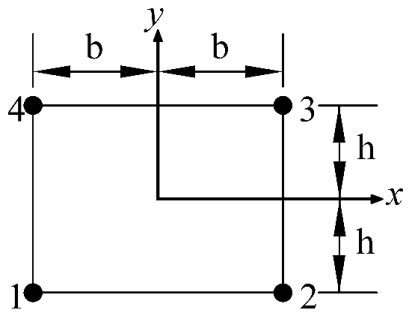

Fig. 4. Four-noded rectangular element

Substituting [*B*] from Eq. (31) and [*D*] from Eq. (6) into Eq. (4) and performing the integrations on the intervals of *x* and *y*, the closed form solution for the stiffness matrix of the element shown in Figure 4 is obtained as:

$$[K_e]=\frac{Et}{24(1-\nu^2)}\times\begin{bmatrix} 4\alpha_1 & 3\alpha_2 & 2\alpha_3 & 3\alpha_4 & -2\alpha_1 & -3\alpha_2 & 4\alpha_5 & -3\alpha_4 \\ & 4\alpha_6 & -3\alpha_4 & 4\alpha_7 & -3\alpha_2 & -2\alpha_6 & 3\alpha_4 & 2\alpha_8 \\ & & 4\alpha_1 & -3\alpha_2 & 4\alpha_5 & 3\alpha_4 & -2\alpha_1 & 3\alpha_2 \\ & & & 4\alpha_6 & -3\alpha_4 & 2\alpha_8 & 3\alpha_2 & -2\alpha_6 \\ & & & & 4\alpha_1 & 3\alpha_2 & 2\alpha_3 & 3\alpha_4 \\ & & Sym. & & & 4\alpha_6 & -3\alpha_4 & 4\alpha_7 \\ & & & & & & 4\alpha_1 & -3\alpha_2 \\ & & & & & & & 4\alpha_6 \end{bmatrix} \tag{32}$$

where $\alpha_1= 2h^2+b^2(1-\nu)$, $\alpha_2= (1+\nu)bh$, $\alpha_3= -4h^2+b^2(1-\nu)$, $\alpha_4= (3\nu-1)bh$, $\alpha_5= h^2-b^2(1-\nu)$, $\alpha_6= 2b^2+h^2(1-\nu)$, $\alpha_7= b^2-h^2(1-\nu)$ and $\alpha_8= -4b^2+h^2(1-\nu)$.

The rectangular element shown in Figure 4 is used as a benchmark problem for validation of the accuracy of the computer code that is described in the next section.

COMPUTER MODELING AND RESULTS

In order to compute the element stiffness matrix of the four-node quadrilateral plane stress element (shown in Figure 2) with normal and reduced numerical integration, a computer program is developed in PYTHON

programming language (version 2.7) (van Rossum and Drake, 2010). The rectangular element shown in Figure 4 is used in order to validate the numerical results obtained by the computer program. The closed form solution of its stiffness matrix has been derived as the Eq. (32). For a rectangular element of b = 6mm, h = 5 mm, t = 1 mm, v = 0.3, and E = 200 GPa, the computer program's evaluation of the stiffness matrix using normal integration is in near agreement with the closed form solution obtained by Eq. (32). The largest difference between the entries of the two matrices is less than 10^{-6} N/mm.

Next, the computer program is extended to solve the eigenvalue problem of Eq. (1), and is used to calculate eigenvalues and eigenvectors of the four-node quadrilateral plane stress elements with different shapes with normal and reduced numerical integration. For each element, the first three eigenvalues are zero; representing the three rigid body motion modes. Subsequently, straining modes of the element is calculated; as presented in the next section.

The Square-Shaped Element and the Mixing Straining Modes

The procedures presented here for splitting the stiffness matrix and application of reduced integration are valid for all four-node quadrilateral plane stress as well as plane strain elements. However, in order to facilitate the observation of the straining modes, only results for rectangular elements are shown here.

First, a 10 mm × 10 mm square-shaped element of t = 1 mm, v = 0.3, and E = 200 GPa is chosen in order to have the straining modes to be drawn. Using normal integration method as well as the reduced integration method, the eigenvalues are obtained for this element. The summary results of eigenvalue analysis using the both aforementioned element integration methods are presented in Table 1. In either case, the first three eigenvalues are near zero, and representing the rigid body motion. The remaining five eigenvalues correspond to the straining modes of the element. Both integration methods result in stiffness matrices which have repeated eigenvalues (algebraic multiplicity). For each one of the repeated eigenvalues, arbitrary sets of linearly independent eigenvalues can be found (Kreyszig, 2011); therefore, the straining modes obtained by PYTHON's eigensolver which are shown in figures 5-10 do not match the straining modes reported in (Bathe, 2014; Pawsey and Clough, 1971). However, these straining modes seem to be a mixture of the straining modes presented in (Bathe, 2014; Pawsey and Clough, 1971). It should be noted that the straining modes are scaled in order to be visible, since multiplying an eigenvector of a matrix by any scalar gives another eigenvector for that matrix.

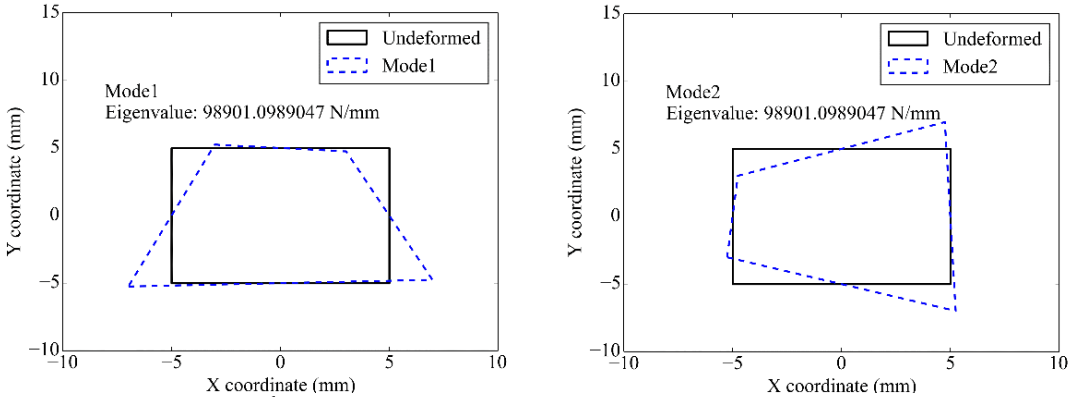

Fig. 5. The 1st and 2nd straining modes of the square-shaped element with normal integration

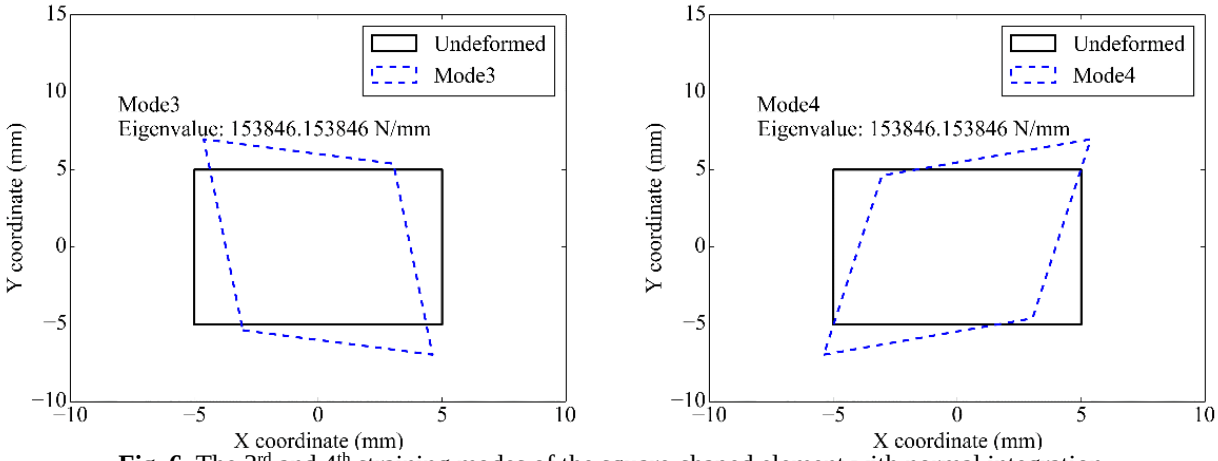

Fig. 6. The 3rd and 4th straining modes of the square-shaped element with normal integration

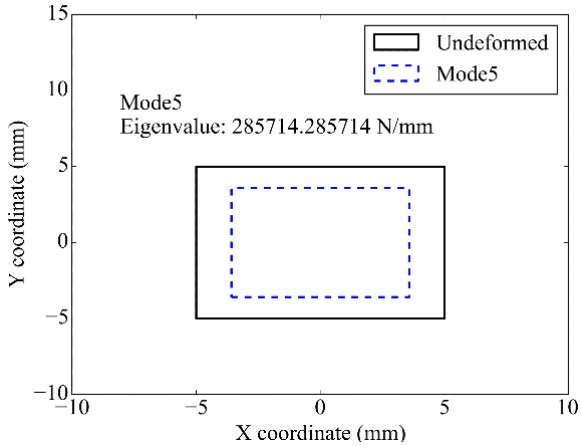

Fig. 7. The 5th straining mode of the square-shaped element with normal integration

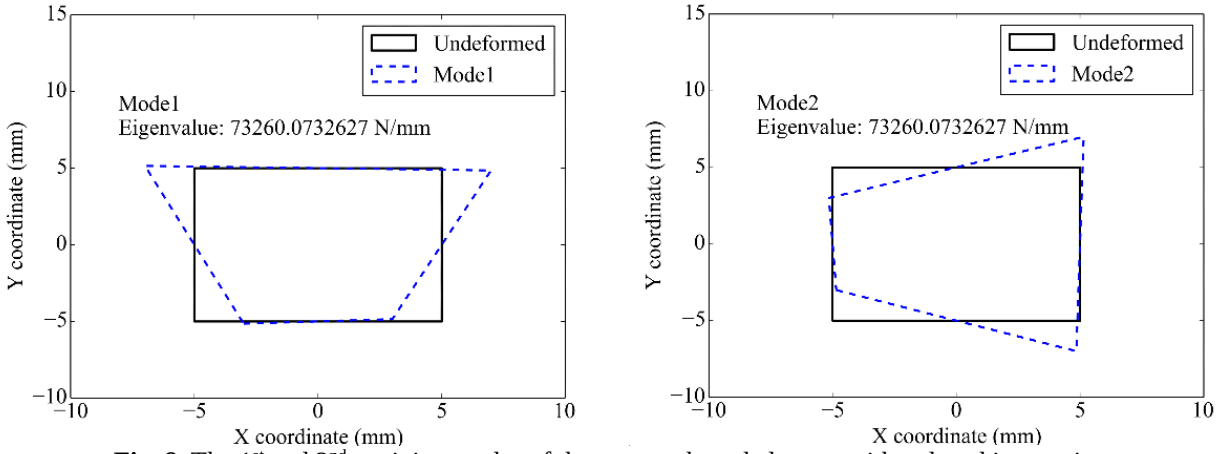

Fig. 8. The 1st and 2nd straining modes of the square-shaped element with reduced integration

Table 1. Eigenvalues obtained for the square-shaped element

Integration Method	**Eigenvalues (N/mm)**							
	1st	**2nd**	**3rd**	**4th**	**5th**	**6th**	**7th**	**8th**
Normal	8×10^{-12}	3.5×10^{-11}	5.1×10^{-11}	98901	98901	153846	153846	285714
Reduced	-2.9×10^{-11}	3.7×10^{-12}	4.4×10^{-11}	73260	73260	153846	153846	285714

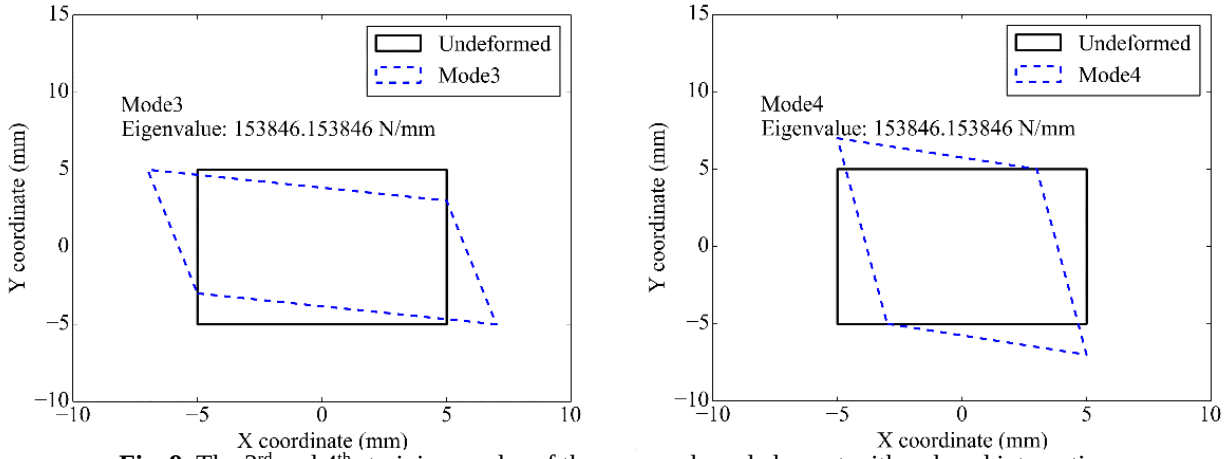

Fig. 9. The 3rd and 4th straining modes of the square-shaped element with reduced integration

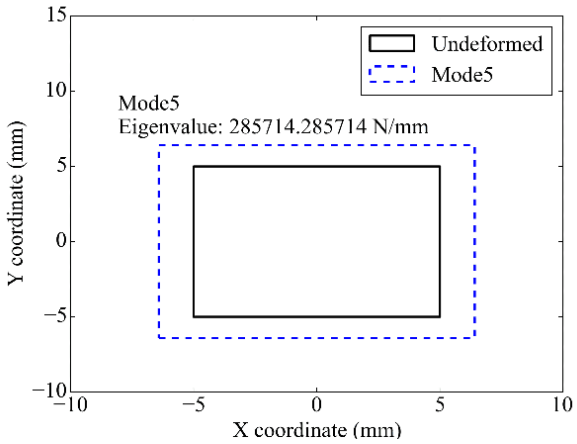

Fig. 10. The 5th straining mode of the square-shaped element with reduced integration

The only strain mode that matches the strain modes reported in (Bathe, 2014; Pawsey and Clough, 1971) is the uniform extension mode, as shown in Figures 7 and 10. The remaining strain modes are mixtures of the strain modes reported in (Bathe, 2014; Pawsey and Clough, 1971); since their corresponding eigenvalues are repeated. Mixing of the straining modes is most visible in the modes 3 and 4. To overcome this problem, and in order to obtain distinct straining modes for the square-shaped element, a slight change in the dimensions of the element is made in a way that the eigenvalues will not be repeated exactly; while the change in the dimensions of the square will be negligible. Thus the width of the element is increased by 0.001 mm. After the above changes, the strain modes obtained are shown in Figures 11-16.

As shown in Figures 11-13, for the element with normal integration, and Figures 14-16 for the element with reduced integration, a slight change in the width of the element resulted in a slight change in the eigenvalues in a way that there are no repeated eigenvalues anymore. Subsequently, the straining modes are not mixed anymore. Strain modes of bending type modes 1 and 2 from Pawsey and Clough (1971), and straining modes of stretching, shear and uniform extension type modes from Bathe (2014) exist in the obtained straining modes. In both cases of normal and reduced integration, a difference of 2.17×10^{-6} percent in eigenvalues corresponding to stretching

and shear straining type modes is enough to cause PYTHON's Eigen solver to find distinct eigenvectors for these eigenvalues; and not to mix the straining modes. Figure 17 shows the eigenvalues corresponding to the straining modes of the square-shaped element, with normal and reduced integration methods.

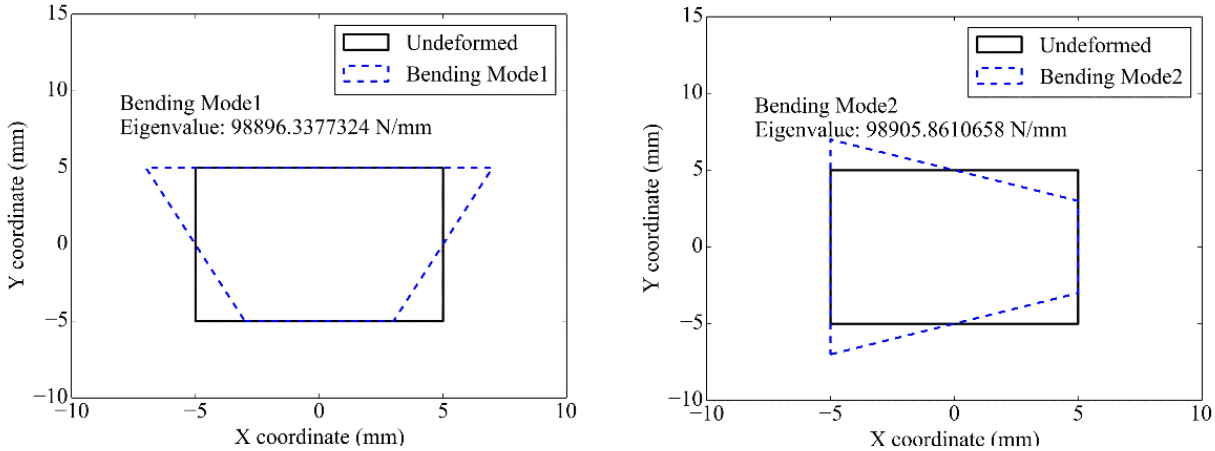

Fig. 11. Bending modes 1 and 2 of the square-shaped element with normal integration

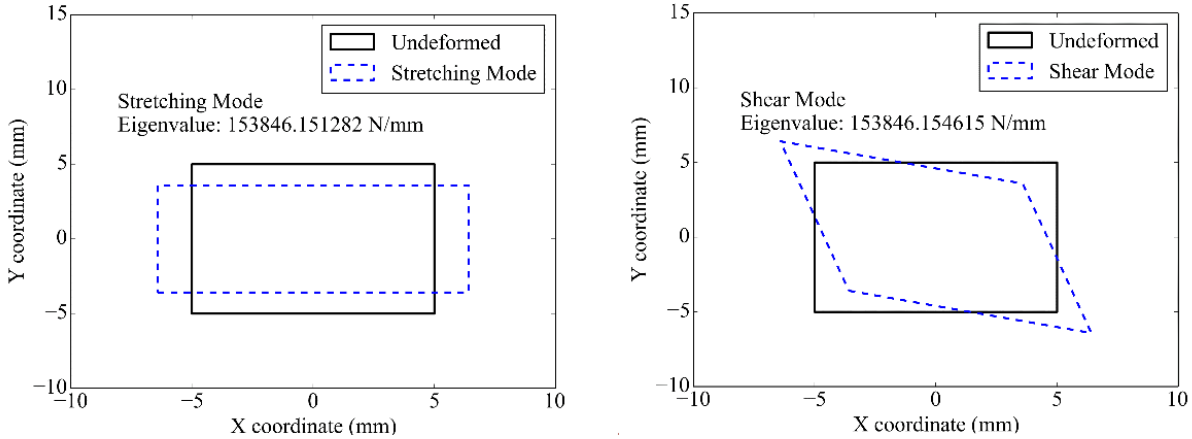

Fig. 12. Bending modes 1 and 2 of the square-shaped element with normal integration

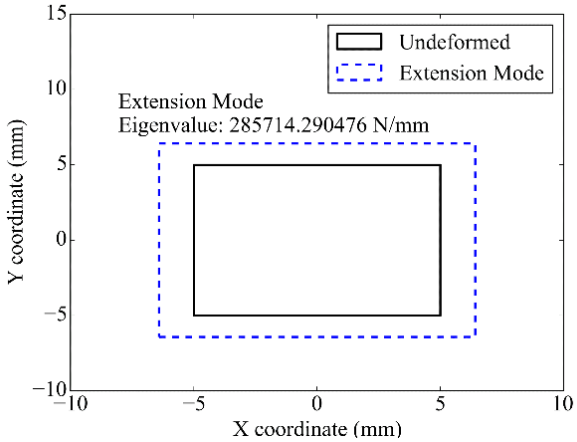

Fig. 13. Extension mode of the square-shaped element with normal integration

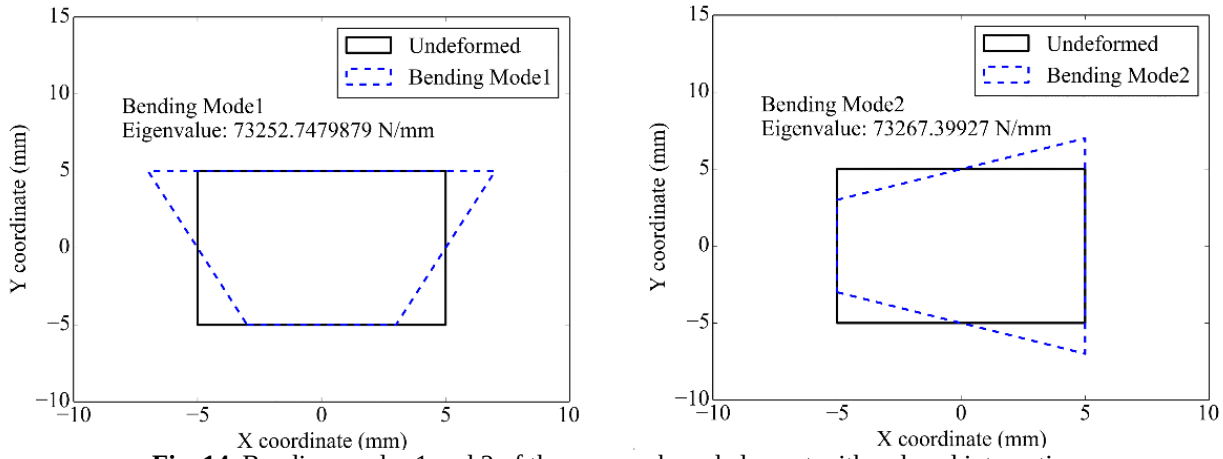

Fig. 14. Bending modes 1 and 2 of the square-shaped element with reduced integration

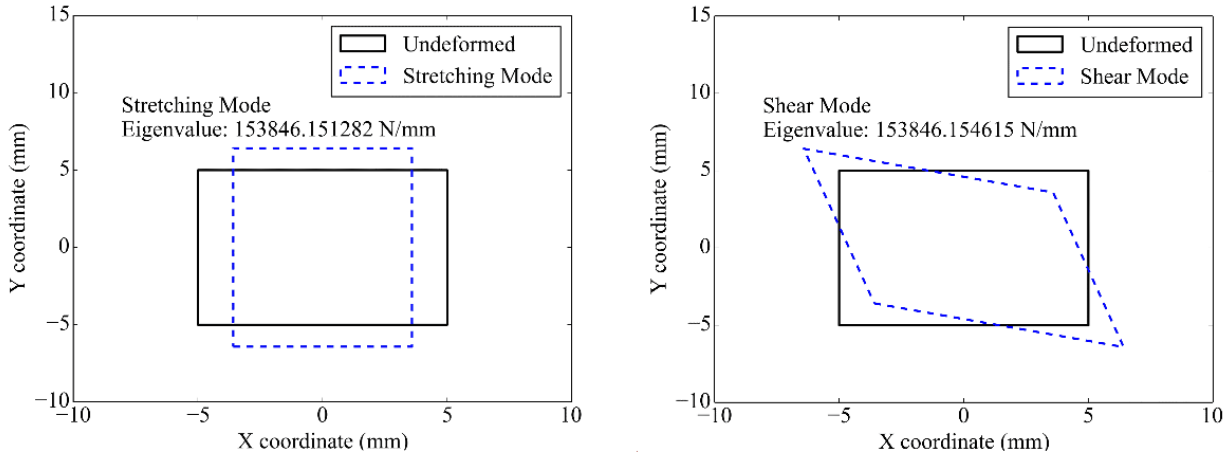

Fig. 15. Stretching and shear modes of the square-shaped element with reduced integration

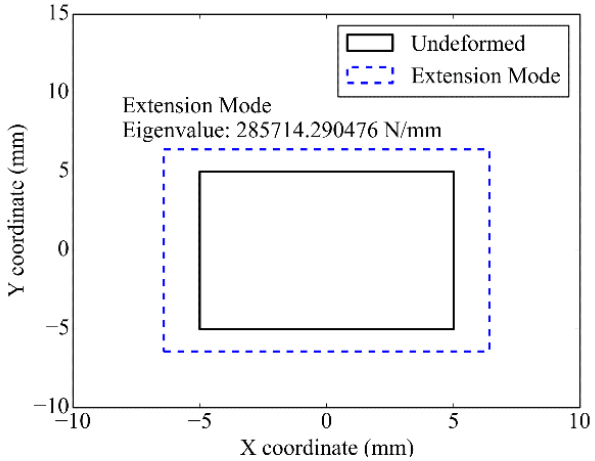

Fig. 16. Extension mode of the square-shaped element with reduced integration

As shown in Figure 17, normal and reduced integration methods result in stiffness matrices which have identical eigenvalues for the stretching, shear, and extension straining modes. On the other hand, the normal integration method results in a

higher value for the eigenvalues corresponding to the bending straining modes. As expected, the interpolation functions of the four-node quadrilateral plane stress element do not allow its edges to bend. Consequently, when this element is subjected to pure bending, the angles between its edges change, and it undergoes shear deformation as well. This produces in an overvaluation of the bending stiffness of the element and consequently leading to have a shear locking condition. The reduced integration method evaluates the shear strain energy of the element by one integration point in the center of the element, where shear strain is zero. As a result, reduced integration resolves the above issue. This is evident from Figure 17, where the reduced integration method gives lower eigenvalues for the bending strain modes.

Rectangular Element with a High Aspect Ratio

To evaluate the effect of aspect ratio of the element on the eigenvalues and the straining modes, a 100 mm × 10 mm size element is chosen. Figures 18-20 illustrate the straining modes obtained for this element using the normal integration method, and Figures 21-23 present the straining modes obtained by the reduced integration method.

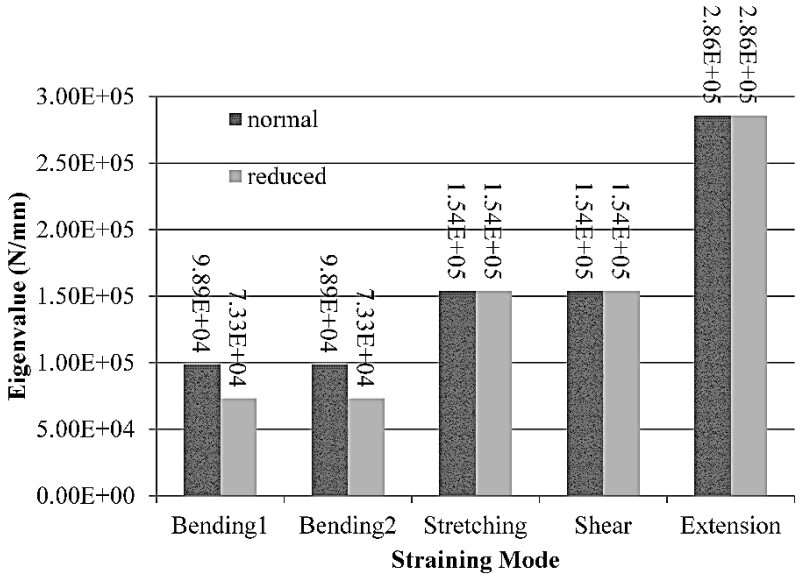

Fig. 17. Eigenvalues of the straining modes in the square-shaped element

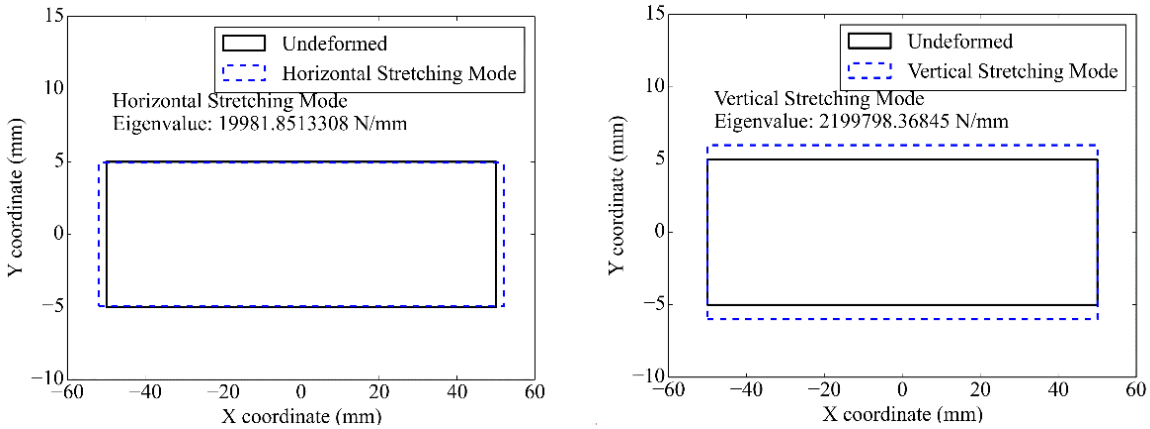

Fig. 18. Stretching modes of the element with aspect ratio of 10, with normal integration

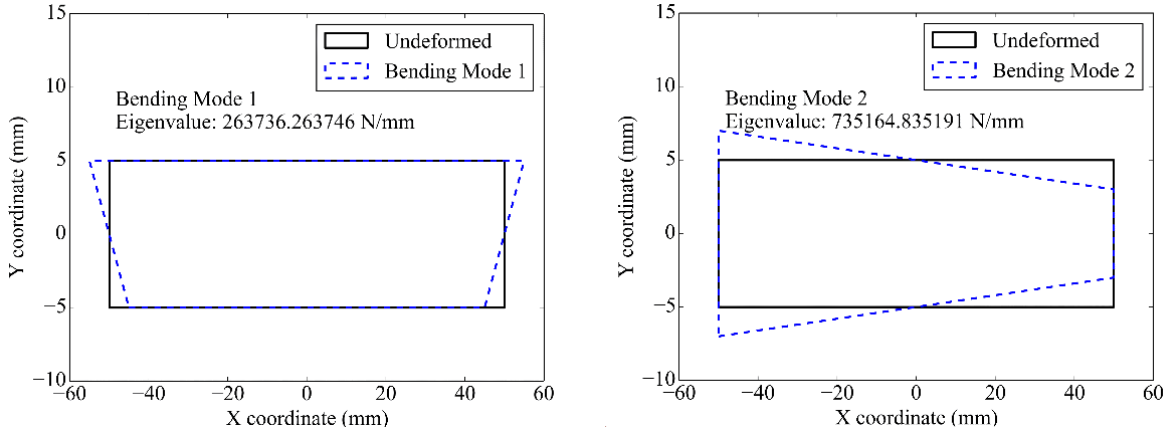

Fig. 19. Bending modes of the element with aspect ratio of 10, with normal integration

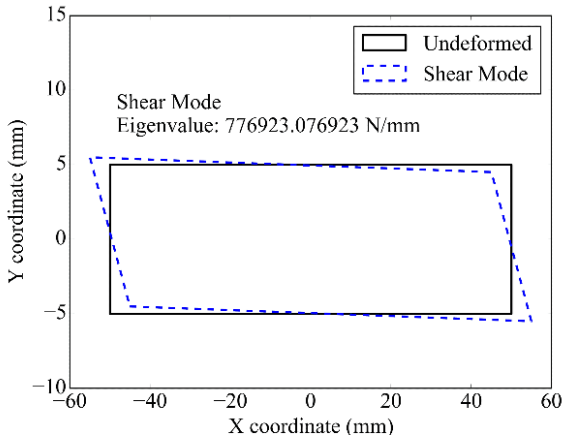

Fig. 20. Shear mode of the element with aspect ratio of 10, with normal integration

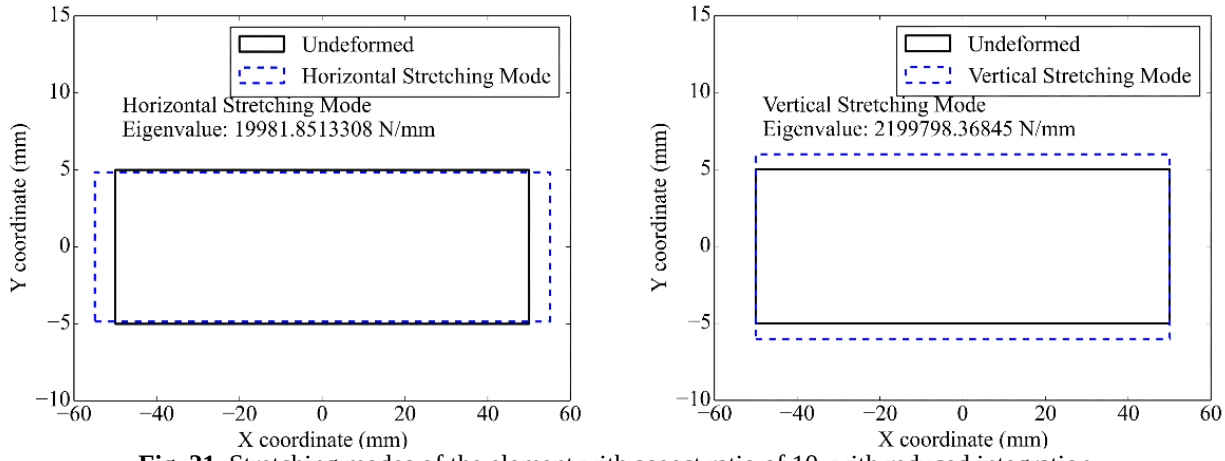

Fig. 21. Stretching modes of the element with aspect ratio of 10, with reduced integration

As illustrated in the aforementioned figures, for the element with the aspect ratio of 10 with normal integration as well as the reduced integration; two bending straining modes, two stretching straining modes, and one shear straining mode are obtained. Figure 24 shows all the eigenvalues corresponding to the straining modes of the element with aspect ratio of 10 using both normal and reduced integration methods.

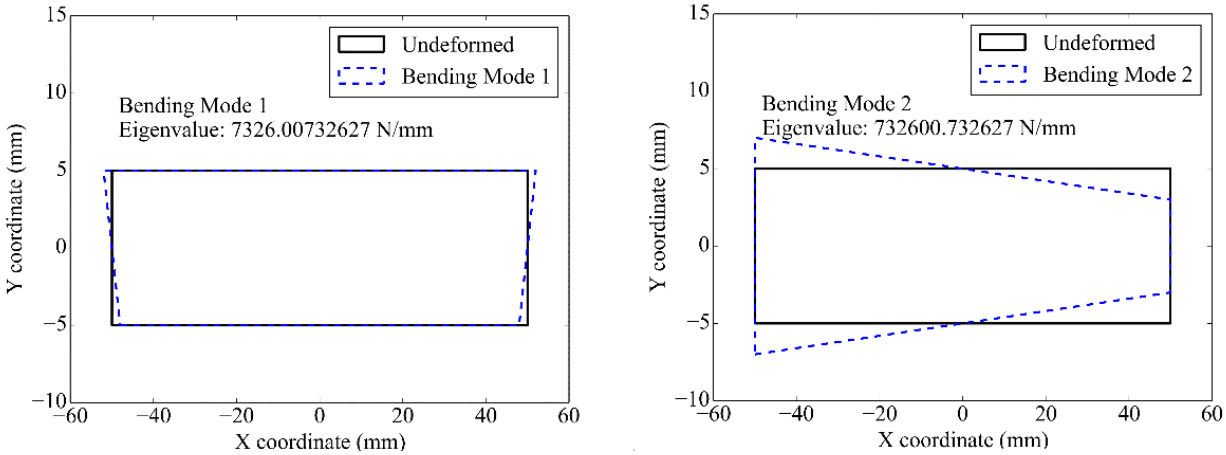

Fig. 22. Bending modes of the element with aspect ratio of 10, with reduced integration

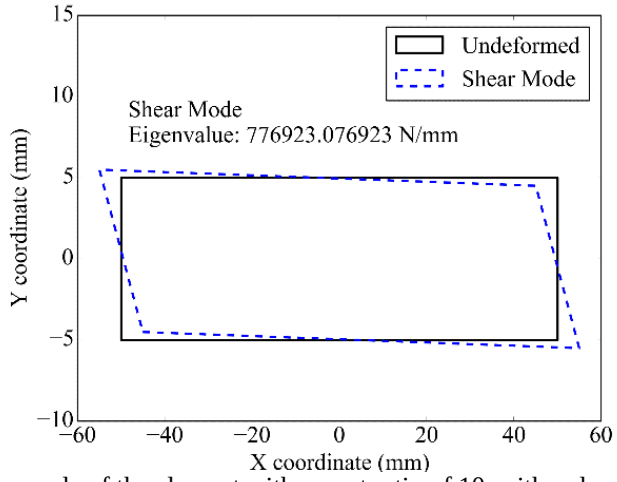

Fig. 23. Shear mode of the element with aspect ratio of 10, with reduced integration

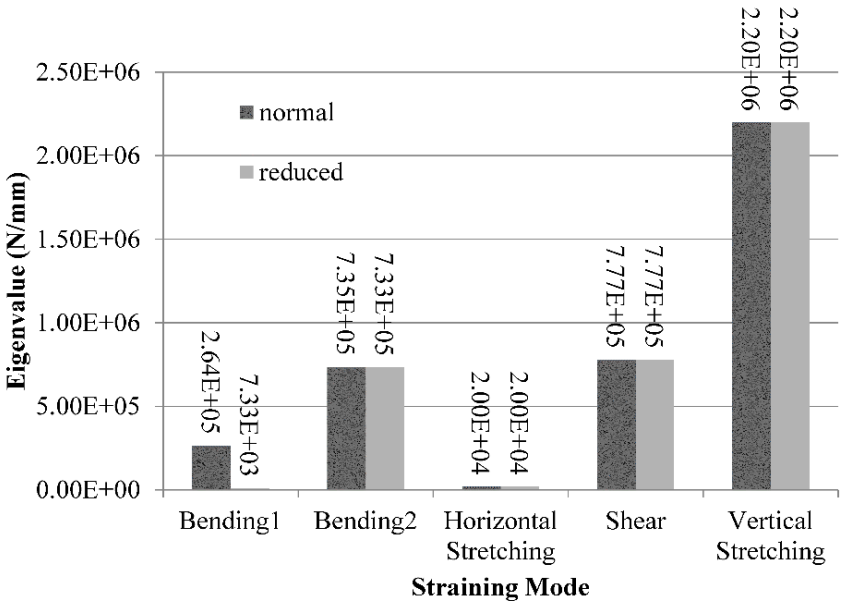

Fig. 24. Eigenvalues of the straining modes of the element with aspect ratio of 10

Normal and reduced integration methods result in stiffness matrices which have different eigenvalues for the bending straining type modes. This difference is much higher for the first bending straining mode. As it was explained earlier, the normal integration method overestimates the bending stiffness of the element. For the element with aspect ratio of 10, this overestimation is highly increased. As it said, this condition is called shear-locking. It is evident from Figure 24 that reduced integration results in a much lower evaluation of the Eigenvalue corresponding to the first bending straining type mode. This is in agreement with the fact that reduced integration (the integrals in the stiffness matrices in Finite Element analysis are evaluated using numerical integration methods.

Numerical integration involves estimating the value of an integral based on evaluated values of the integrated function at certain Gauss points inside the integration domain. While the normal way of performing the numerical integration and in order to have an accurate estimation of the integrals, would be to use sufficient number of integration points, reduced integration means separating part of the stiffness matrix that represents the shear strain energy of the element, and using a lower order of integration (less integration points) to perform the numerical integration on that part.) is an effective way to prevent shear-locking. For the element with aspect ratio of 10, the extension straining type mode is replaced by a vertical stretching mode. The two flexural modes of Bathe (2014) are not observed among the straining modes obtained in this study; while the two bending modes of Pawsey and Clough (1971) are observed instead.

CONCLUSIONS

A method of applying the reduced integration method to quadrilateral plane stress elements is presented. Subsequently, a computer program is developed for calculating stiffness matrices of quadrilateral plane stress elements using normal and reduced integration methods. Furthermore, for the case of rectangular shaped element, a closed form solution is presented for the stiffness matrix. For a rectangular element, the developed computer program delivered exactly the same results as obtained by the closed-form solution.

Also for particular square shaped element and by means of the developed program, straining modes are obtained by performing an eigenvalue analysis on the stiffness matrices obtained using both normal and reduced integration methods. The stiffness matrix of this particular square shape geometry, revealed repeated eigenvalues with mixed straining modes. However, it was illustrated that by making a slight change in the geometry, the problem of having repeated eigenvalues is avoided and distinct bending, stretching, shear, and extension straining modes are attained.

The integration methods have no effect on the straining modes. However, they do affect the eigenvalues. The straining modes and the corresponding eigenvalues represent special cases of loading applied to elements, where the force vector and the nodal deformation vectors are scalar multiples of each other. The magnitude of the eigenvalue obtained for each straining mode represents the stiffness of the element against that specific deformation shape. From an Eigen-analysis perspective, this research papers observes the connection between higher eigenvalues for bending straining modes and the conditions that are known to lead to shear-locking. For the bending straining modes, the normal integration method results in higher values for eigenvalues compared with the bending eigenvalues obtained by the reduced integration method. For the element with aspect ratio of 10, this difference is increased

dramatically. This observation confirms the occurrence of shear-locking, which is a common condition for elements having high aspect ratios under pure bending loads.

The analytical methods derived and applied in this research are applicable to finite element calculations using quadrilateral plane stress and plane stress elements with reduced integration.

REFERENCES

Adam, C., Bouabdallah, S., Zarroug, M. and Maitournam, H. (2014). "Improved numerical integration for locking treatment in isogeometric structural elements, Part I: Beams", *Computer Methods in Applied Mechanics and Engineering*, 279, 1-28.

Adam, C., Bouabdallah, S., Zarroug, M. and Maitournam, H. (2015). "Improved numerical integration for locking treatment in isogeometric structural elements. Part II: Plates and shells", *Computer Methods in Applied Mechanics and Engineering*, 284, 106-137.

Arnold, D. and Brezzi, F. (1997). "Locking-free Finite Element methods for shells", *Mathematics of Computation of the American Mathematical Society*, 66(217), 1-14.

Bathe, K.J. (2014). *Finite Element Procedures*, 2nd Edition, K.J. Bathe, Watertown, MA, USA.

Bletzinger, K.U., Bischoff, M. and Ramm, E. (2000). "A unified approach for shear-locking-free triangular and rectangular shell Finite Elements", *Computers and Structures*, 75(3), 321-334.

da Veiga, L. B., Lovadina, C., and Reali, A. (2012). "Avoiding shear locking for the Timoshenko beam problem via isogeometric collocation methods", *Computer Methods in Applied Mechanics and Engineering*, 241, 38-51.

Fallah, N., Parayandeh-Shahrestany, A. and Golkoubi, H. (2017). "A Finite Volume formulation for the elasto-plastic analysis of rectangular Mindlin-Reissner plates, a non-layered approach", *Civil Engineering Infrastructures Journal*, 50(2), 293-310.

Garcia-Vallejo, D., Mikkola, A.M. and Escalona, J.L. (2007). "A new locking-free shear deformable Finite Element based on absolute nodal coordinates", *Nonlinear Dynamics*, 50(1-2), 249-264.

Javidinejad, A. (2012). "FEA practical illustration of mesh-quality-results differences between structured mesh and unstructured mesh", *ISRN Mechanical Engineering*, Volume 2012, Article ID 168941, 7 pages, doi:10.5402/2012/168941.

Kanok-Nukulchai, W., Barry, W., Saran-Yasoontorn, K. and Bouillard, P. H. (2001). "On elimination of shear locking in the element-free Galerkin method", *International Journal for Numerical Methods in Engineering*, 52(7), 705-725.

Kreyszig, E. (2011). *Advanced engineering mathematics*, 10th Edition, John Wiley & Sons, New Jersey, USA.

Liu, G.R. and Quek, S.S. (2014). *The Finite Element method, A practical course*, 2nd Edition, Butterworth–Heinemann, Oxford, UK.

Logan, D.L. (2012). *A first course in the Finite Element method*, 5th Edition, Global Engineering, Stamford, CT, USA.

Nguyen-Thanh, N., Rabczuk, T., Nguyen-Xuan, H. and Bordas, S.P. (2008). "A smoothed Finite Element method for shell analysis", *Computer Methods in Applied Mechanics and Engineering*, 198(2), 165-177.

Nguyen-Xuan, H., Liu, G.R., Thai-Hoang, C.A. and Nguyen-Thoi, T. (2010). "An edge-based smoothed Finite Element method (ES-FEM) with stabilized discrete shear gap technique for analysis of Reissner-Mindlin plates", *Computer Methods in Applied Mechanics and Engineering*, 199(9-12), 471-489.

Pagani, M., Reese, S. and Perego, U. (2014). "Computationally efficient explicit nonlinear analyses using reduced integration-based solid-shell Finite Elements", *Computer Methods in Applied Mechanics and Engineering*, 268, 141-159.

Pawsey, S.F. and Clough, R.W. (1971). "Improved numerical integration of thick shell Finite Elements", *International Journal for Numerical Methods in Engineering*, 3(4), 575-586.

Pugh, E.D.L., Hinton, E. and Zienkiewicz, O.C. (1978). "A study of quadrilateral plate bending elements with reduced integration", *International Journal for Numerical Methods in Engineering*, 12(7), 1059-1079.

Reddy, J.N. (1997). "On locking-free shear deformable beam Finite Elements", *Computer Methods in Applied Mechanics and Engineering*, 149(1-4), 113-132.

Reddy, J.N. (2006). *An introduction to the Finite Element method*, 3rd Edition, McGraw Hill, New Jersey, USA.

Rezaiee-Pajand, M. and Yaghoobi, M. (2012). "Formulating an effective generalized four-sided element", *European Journal of Mechanics-A/Solids*, 36, 141-155.

Rezaiee-Pajand, M. and Yaghoobi, M. (2013). "A free of parasitic shear strain formulation for plane

element", *Research in Civil and Environmental Engineering*, 1, 1-27.

Rezaiee-Pajand, M. and Yaghoobi, M. (2014). "A robust triangular membrane element", *Latin American Journal of Solids and Structures*, 11(14), 2648-2671.

Rezaiee-Pajand, M. and Yaghoobi, M. (2015). "Two new quadrilateral elements based on strain states", *Civil Engineering Infrastructures Journal*, 48(1), 133-156.

Rezaiee-Pajand, M. and Yaghoobi, M. (2017). "A hybrid stress plane element with strain field", *Civil Engineering Infrastructures Journal*, 50(2), 255-75.

van Rossum, G. and Drake, F.L. (2010). "The Python Language Reference", Python Software Foundation, from https://docs.python.org/release/2.7/reference/index.html

Videla, L., Baloa, T., Griffiths, D. V. and Cerrolaza, M. (2007). "Exact integration of the stiffness matrix of an 8-node plane elastic Finite Element by symbolic computation", *Numerical Methods for Partial Differential Equations*, 24(1), 249-261.

Walentyski, R.A. (2008). "On exact integration within an isoparametric tetragonal Finite Element", *International Conference of Numerical Analysis and Applied Mathematics, AIP Conference Proceedings*, 936, 582-585.

Zienkiewicz, O.C., Taylor, R.L. and Too, J.M. (1971). "Reduced integration technique in general analysis of plates and shells", *International Journal for Numerical Methods in Engineering*, 3(2), 275-290.